IFSCC 2025 full paper (IFSCC2025-623)

Senescent melanocytes as a key driver of human skin aging

Morgan Dos Santos[2], Kilian Laho[2], Sandrine Heraud[2], Amélie Thépot[2], Marion Renault[1], Juliette Sage[1], Olivier Jeanneton[1], Jocelyne Franchi[1], Carine Nizard[1], Karl Pays[1], Laure Crabbe Vert[1]

[1] LVMH RECHERCHE, 45804 Saint Jean de Braye, France
[2] LABSKIN CREATIONS, 69004, Lyon, France

1. Introduction

Melanocytes are a group of cells present in the human body that originate from neural crest embryonic cells. In human skin, melanocytes are located at the *stratum basale* of the the epidermis and present in hair follicules, where they are able to procude photoprotective melanin pigments, which are transferred to adjacent keratinocytes **[1]**. Mature melanocytes are fusiform, with dendrites that extend to associate with surrounding keratinocytes. In the epidermis, melanocytes reside in the basal layer at a ratio with keratinocytes ranging from 1:5 to 1:10, but they connect with an average of 30 to 40 keratinocytes, forming the so-called melanin unit described in the 60s **[2]**. Melanocytes are long-lived cells that are found mainly in a quiescent state within the tissue. Melanocytes comprise approximatively 1-3% of epidermal cells and are thus the second most numerous epidermal cell type after keratinocytes **[3]**. However their distribution and proliferation depends on the environment, mainly UV irradiations, and factors secreted by keratinocytes and fibroblasts **[1]**.

Aging can also impact melanocyte density, as it was estimated that after 30 years of age, 10-20% of epidermal melanocytes are lost every decade **[4]**. Skin aging is the result of a gradual functional decline of the tissue properties. At the cellular level, aging was first described upon the discovery that somatic cells possess a finite capacity for cell division, after which they enter an irreversible growth arrest known as cellular senescence. Senescent cells have a very special “signature”: they are unable to proliferate, they are resistant to the cell death pathway called apoptosis, and most importantly they secrete factors that can negatively impact their surroundings. Like a disturbing neighbour, senescent cells can stress the nearby cells, promote inflammation and tissue deterioration through extracellular matrix degradation. It was recently shown that senescent melanocytes accumulated with age in human skin punch biopsies, negatively affecting the surrounding keratinocytes **[5]**. Despite this important finding, very few publications explore the impact of senescence on melanocytes, the consequences on neighbouring cells and on melanin production and skin pigmentation. Yet, pigmentation spots typically occur with age in chronically sun-exposed skin as a result of irregularities in melanocyte distribution, enhanced melanogenic signaling, and decrease melanosome removal **[6]**. To

what extend melanocyte senescence can play a role in the occurrence of photo-induced age spots is still unclear.

Here, we aimed to identify the molecular, cellular and tissular consequences of human normal senescent melanocytes using a combination of approaches based on a variety of *in vitro* models ranging from 2D to advanced 3D skin models. This work allowed us to identify key pathways triggering pigmentation disorders that derive from integrating senescent melanocytes in these human skin models. We also demonstrate that our model can be used to identify active ingredients that proven efficient against senescence-induced cellular and tissular dysfunctions.

2. Materials and Methods

2.1 Ethical considerations and human cutaneous cell isolation

Human skin tissues were collected from surgical discard from anonymous healthy donors. Surgical residues were anonymized, and written informed consent was obtained from the patients in accordance with the ethical guidelines from Lyon University Hospital (Hospice Civils de Lyon) and approved by ethical committee of the Hospices Civils de Lyon according to the principles of the Declaration of Helsinki and Article L. 1243-4 of the French Public Health Code. All the samples used in this study belong to a collection of human skin samples declared to the French Research Ministry (Declaration no. DC-2024-6232 delivered to LabSkin Creations, Lyon, France). Primary cultures of human fibroblasts, keratinocytes, and melanocytes were established from healthy skin biopsy obtained from an infant donor (<5 years old) or an adult donor (>40 years old). Normal human epidermal keratinocytes (NHEKs), melanocytes (NHEMs), and dermal fibroblasts (NHDFs) were isolated from human skin.

2.2 UV Irradiation and Induction of Senescence in NHEM

NHEM at 70–80% confluency were rinsed twice with phosphate-buffered saline (PBS) and exposed to UVA and UVB irradiation using a calibrated UV irradiator. The cells were irradiated with a dose of UVA and UVB ranging from 0.1-5.0 and 100–400 mJ/cm², respectively, previously optimized to induce cellular senescence without excessive cytotoxicity. Immediately following irradiation, cells were replenished with fresh medium and irradiated for 4 consecutive days, during which they were monitored for senescence-associated morphological changes.

2.3 Co-culture of NHEK and Senescent NHEM

Senescent NHEM were trypsinized and seeded together with NHEK at a 1:3 ratio (NHEM:NHEK) in a 6-well plate system, depending on the assay type. Co-cultures were maintained in an optimized medium to support both cell types. Co-culture was maintained for 3–7 days for downstream analyses.

2.4 3D pigmented reconstructed skin engineered

3D full-thickness reconstructed skin model was obtained by culturing NHDF in a scaffold made of collagen, glycosaminoglycans and chitosan (LabSkin matriX^{TM}, Lyon, France) during 21 days under optimized cell culture conditions for ECM neo-synthesis as previously described[7]. NHEK and UV-induced senescent NHEM were then spotted by bioprinting on the top of the dermal equivalent constructs and raised at the air/liquid interface to allow the formation of the epidermal compartment. Non irradiated NHEM were used as negative control.

For whitening product evaluation, 3D reconstructed skin samples were systematically treated systemically starting from day 10 till the end of the culture. Treatments were renewed three times a week. At the end of the culture, tissue constructs were harvested and fixed for histological and immunohistological analysis, respectively. Skin equivalent samples harvested at day 42 of total cell culture were immediately fixed in neutral buffered formalin 4% (Diapath) for 24 h and embedded in paraffin or in OCT compound and frozen at −80°C, for histological and

immunohistological analysis, respectively. For each cell culture condition and analysis, 3D skin equivalents were produced in triplicate.

2.5 Histological analysis

Haematoxylin-phloxin-saffron staining

To evaluate the global cutaneous structure of samples, haematoxylin-phloxin-saffron (HPS) staining was performed. Paraffin sections of 5µm of each condition were cut. After dewaxing and rehydration, the samples were stained with HPS. After rinsing, the sections were dehydrated before the mounting of the slides with a hydrophobic mounting medium.

Warthin Starry staining

To evaluate melanin synthesis, Warthin Starry silver staining was performed. After deparaffinization and rehydration sections were incubated with a silver nitrate solution 6 % for 20 minutes following Suppliers' kit instruction (Merck). The development of the silver was stopped in a washing step with water. Then, sections were incubated with hydroquinone and gelatine mixture. This step allowed the development of melanin granules in dark brown to black and the counterstaining of skin equivalent sections in yellow to orange.

2.6 Melanin content

To quantify melanin content, NHEM, cultured either alone or in co-culture with NHEK, were harvested by trypsinization, washed with PBS, and pelleted by centrifugation at 1000 rpm for 10 minutes. Cell pellets were lysed with 1 M potassium hydroxide (KOH) and incubated at 45°C for 1 hour to solubilize melanin. Samples were then cooled to room temperature, and absorbance was measured at 405 nm using a microplate reader. A standard curve was generated using synthetic melanin (Sigma-Aldrich) dissolved in 1 M KOH to estimate absolute melanin concentration. Melanin content was normalized to total cell number to account for differences in cell density. All measurements were performed in technical triplicates.

2.7 Immunocytological analysis

For immunocytochemical analysis, UV-induced senescent NHEM, cultured either alone or in co-culture with NHEK, were fixed in 4% paraformaldehyde for 15 minutes at room temperature. After permeabilization with 0.1% Triton X-100 for 10 minutes, cells were blocked in 5% BSA for 1 hour and incubated overnight at 4°C with primary antibodies against $p16^{INK4a}$,Melan-A and LC3B. Following PBS washes, cells were incubated with Alexa 488/568 Fluor-conjugated secondary antibodies for 1 hour at room temperature in the dark, and nuclei were counterstained with DAPI. Coverslips were mounted using ProLong™ Gold Antifade and imaged using a fluorescence omicroscope with optimised acquisition settings. For co-cultures, Melan-A staining was used to distinguish melanocytes from keratinocytes. Quantitative analysis of marker expression, including $p16^{INK4a}$, LC3b, and Melan-A positivity, was performed using ImageJ software across nine randomly selected fields per condition. Negative controls without primary antibody was included to confirm antibody specificity.

2.8 Immunohistological analysis

For immunohistochemistry on paraffin sections, after heat-mediated antigen retrieval treatment, non-specific binding was blocked in PBS containing 4% of BSA. Sections were then incubated with the primary antibodies against $p16^{INK4a}$ and Melan-A, diluted at optimal concentration in PBS/BSA 4%, overnight at room temperature. After incubation for 1 h with EnVision anti-mouse/rabbit-HRP secondary antibody (Dako EnVision$^+$, HRP) and apply DAB$^+$ substrate solution to the sections to reveal the colour of the antibody staining. Counterstain slides by immersing them in 25% Harris Haematoxylin counterstaining solution. As a negative control, primary antibody was replaced by the corresponding IgG class.

2.9 Microscopic image acquisition and analysis

Immunostained specimens were observed using an Axio Observer A1/D1 optical microscope (Zeiss), and images were captured using AxioCam HRc (Zeiss) and ZEN 2 pro (Zeiss). Sixteen-bit images were saved in an uncompressed tagged image file format (tiff). Nine representative images were captured for each condition in the same manner.
For the markers of interest, positively red or green stained-tissue/cells areas were automatically detected and segmented from other pixels. Images were then converted in binary images, treated by mathematical morphology and sieved for isolating the regions of interest. The surface area of interest was measured automatically. Data were normalized by the total number of cells or the epidermal/dermal total surface area. Data are expressed in percentage of density.

2.10 Statistical analysis

For all data, the statistical significance was assessed running one-way Anova using Dunnett test for multiple comparison, and statistically significant differences are indicated by asterisks as follows: *P < 0.05, **P < 0.01, ***P < 0.001, ****P < 0.0001

3. Results

3.1 Mild and repeated doses of combined UVA+UVB irradiations induce senescence in a *mono*culture of *NHEM*

NHEM *were exposed daily for 4 consecutive days to different ratios of* combined *UVA and UVB to determine the conditions that induced the expression of the senescent marker p16^{INK4A} without affecting cellular viability. Table 1 summarizes the irradiation conditions that were selected for the study.*

Name	UVA/UVB ratio	Daily UVA (J/cm^2)	Daily UVB (mJ/cm^2)	Cumulative UVA (J/cm^2)	Cumulative UVB (mJ/cm^2)
UVA+UVB 1	33	5	150	20	600
UVA+UVB 2	1	0.4	400	1.6	1600

Table 1. *Irradiation conditions used in the study*

p16^{INK4A} immunostaining revealed that one day following the last UV exposure, both irradiation conditions resulted in increased p16-positive NHEM (+102% and +97%, respectively). 4 days post irradiation, the percentage of p16-positive NHEM was either stable or further increased, suggesting that these cells engaged the senescence pathway (Figure 1a-b). This resulted in a marked increase in melanin content that was observed at both time points in the culture (Figure 1c).

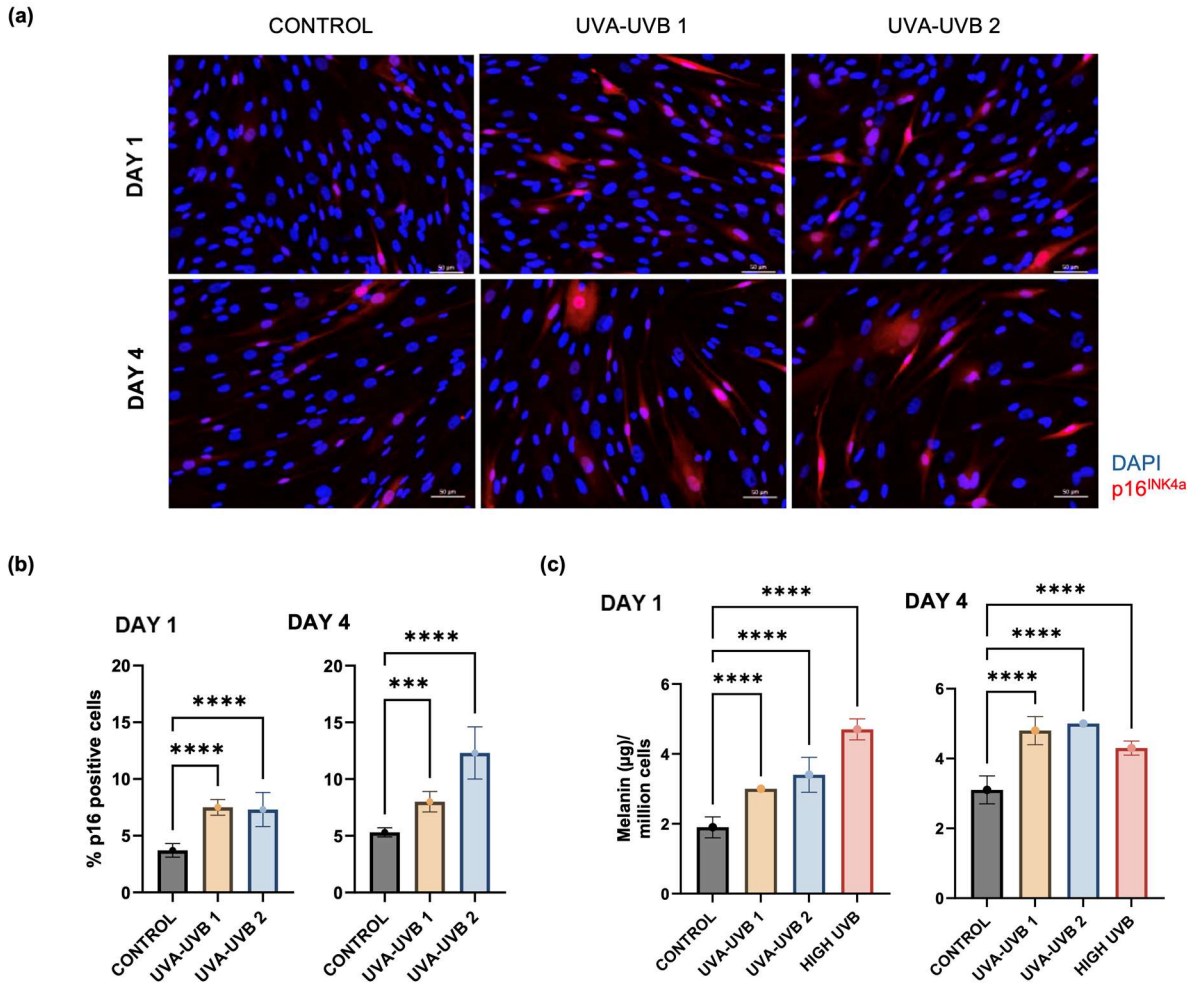

Figure 1. Immunocytostaining of the regulation of senescence-associated protein $p16^{INK4a}$ in NHEM following UVA/UVB exposure. **(a)** Representative immunofluorescence images showing p16 expression (red). Cell nuclei are counterstained with DAPI (blue). **(b)** Quantification by image analysis of (a) 1 day or 4 days post $UV_{A/B}$ exposure. **(c)** Quantification of melanin content in the indicated conditions 1 day or 4 days post exposure.

3.2 $p16^{INK4A}$ -positive NHEM impacts senescence of native NHEK in 2D co-culture model

We next investigated the paracrine impact of UV-induced senescent melanocytes on keratinocytes, by using an *in-vitro* co-culture system. One day following the last irradiation, melanocytes were trypsinized and co-seeded with NHEM for seven days before fixing the cells for analysis. Melanocytes were identified within the co-culture using the Melan-A marker, which allowed us to determine the levels of additional markers, individually, in both cell types. Even after 8 days of culture following the final UVA/UVB exposure, $p16^{INK4A}$-positive NHEM remained elevated, showing a 79% to 216% increase compared to unexposed controls (Figure 2a-b). When co-seeded with senescent NHEM, the number of $p16^{INK4A}$-positive NHEK also raised to 70% and 104% with both UVA/UVB doses initially applied on NHEM. This result confirmed the capacity of the senescent signal to spread to neighbouring cells. In addition, the co-culture with UV-induced senescent NHEM contained higher levels of melanin compared to the control groups (Figure 2c). UV-induced senescent NHEM can therefore overproduce melanin long after their UV exposure.

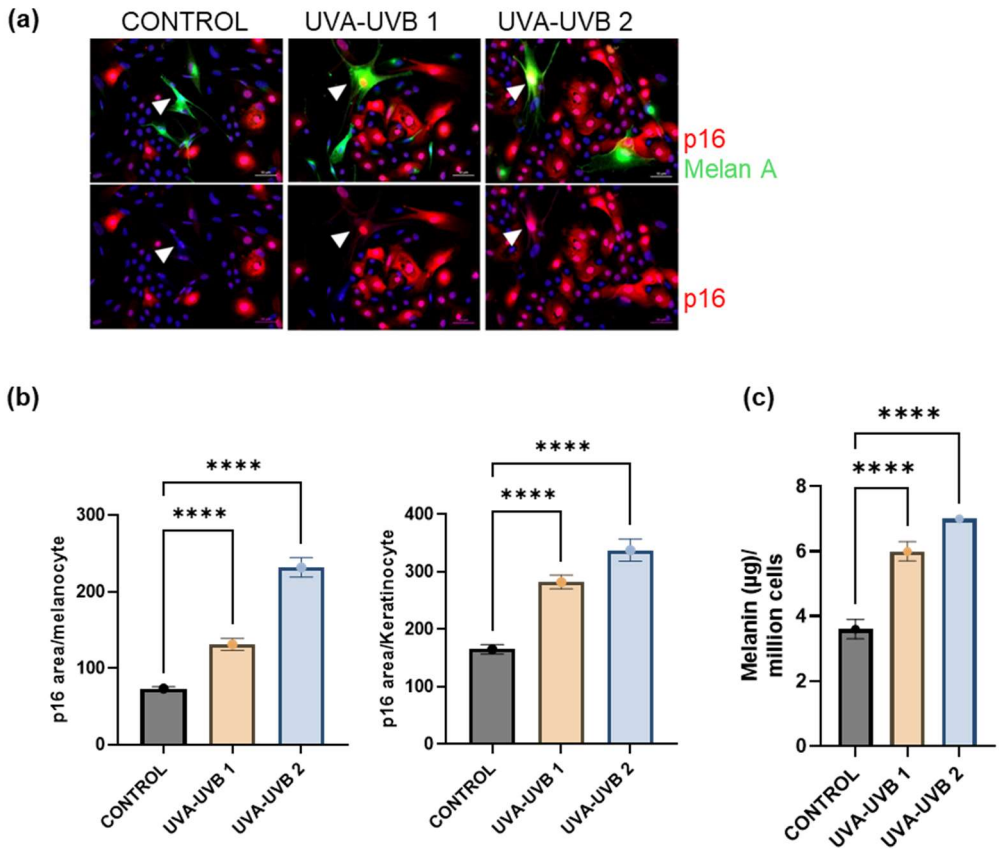

Figure 2. Immunocytostaining of the regulation of senescence-associated protein $p16^{INK4a}$ in co-culture of UVA/UVB-induced senescence NHEM with native NHEK. **(a)** Representative immunofluorescence images showing p16 (red) and Melan-A (green) expression. Cell nuclei are counterstained with DAPI (blue). **(b)** Quantification of (a) p16 levels expressed in NHEM (left graph) and NHEK (right graph) from the co-culture. **(c)** Quantification of melanin content in NHEM/NHEK co-culture.

3.3 $p16^{INK4A}$ -positive NHEM *activates autophagy pathway in NHEK* in co-culture

Recently, it was shown that the process of UVB-induced senescence of melanocytes involved impairment of proteasome activity and exacerbated autophagic activity *[6]*. Autophagy is also known to play a specific role in the synthesis, degradation, and transport of the melanosomes, and as such could be involved in pigmentation disorders *[6]*. We therefore assessed autophagy activation in our NHEM/NHEK co-culture model using the expression of LC3B, a major actor in the pathway. We confirmed that LC3B levels were increased following a treatment with rapamycin, a pharmaceutical drug known to activate autophagy (Figure 3a-b). We observed a similar increase in LC3B expression in both NHEM and NHEK from the co-culture with UV-induced senescent NHEM (Figure 3a-b). These results suggest that UV exposure induced autophagy in melanocytes, as previously shown, but most importantly that this signal could spread to neighbouring native keratinocytes.

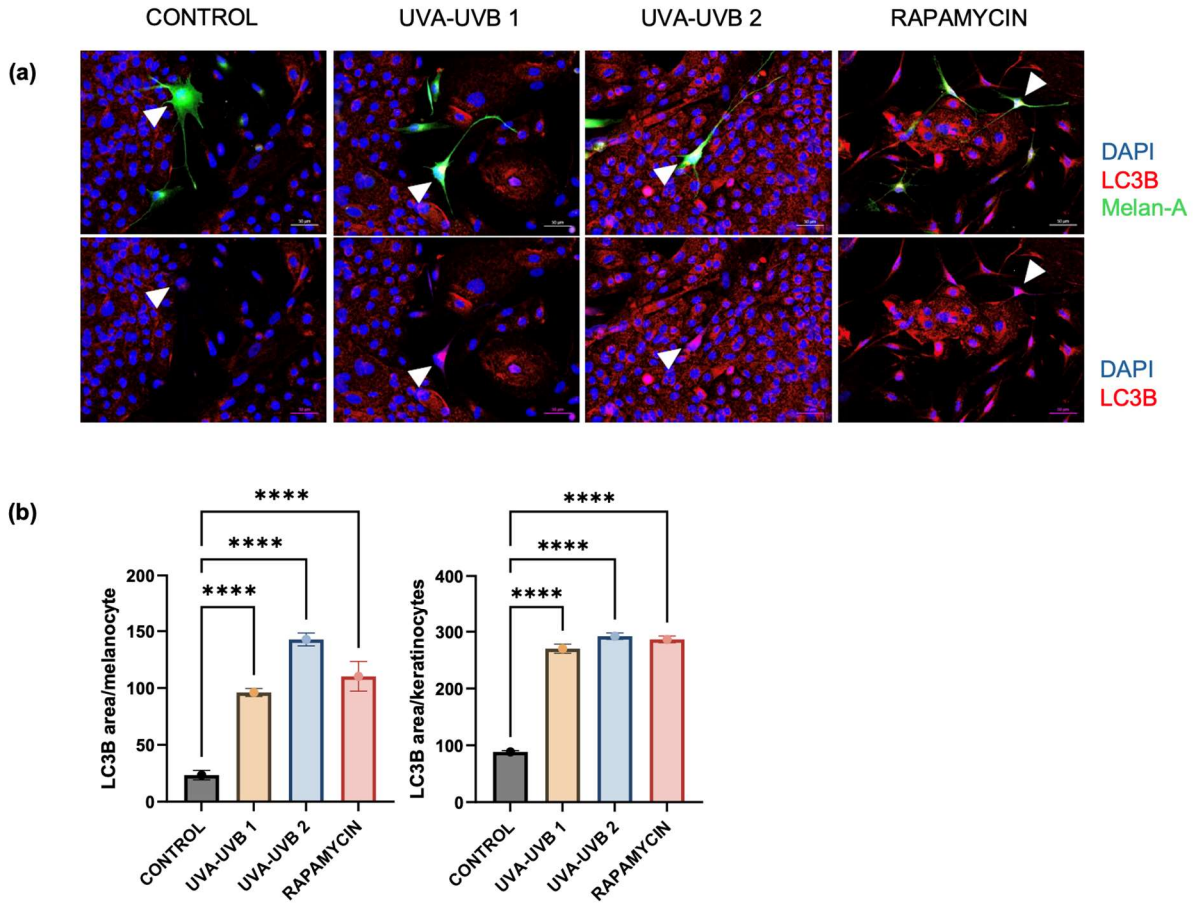

Figure 3. Immunocytostaining of the autophagy-associated protein LC3b in the co-culture of UVA/UVB senescence-induced NHEM with NHEK. **(a)** images showing p16 expression (red) and the melanocyte marker Melan-A (green). Cell nuclei are counterstained with DAPI (blue). **(b)** Quantification of (a). LC3b levels are quantified in NHEM (left graph) and NHEK (right graph) from the UVA/UVB-induced senescence NHEM / native NHEK co-culture.

3.3 A whitening molecule can protect melanocytes and keratinocytes from senescence and melanin production in 2D co-culture

Next, we investigated whether a whitening ingredient could protect cells against UV-induced senescence and pigmentation. Treatment was performed in two stages, first during the preparation of UV-induced senescent melanocytes, and second during the 2D co-culture (detailed in the method section). We observed a strong reduction in $p16^{INK4A}$-positive NHEM and NHEK, which correlated with a reduction in LC3B signal in both cell types (Figure 4a-b). These results suggest that the ingredient protected against UV-induced senescence in melanocytes, and protected against the spreading of the senescence signal in the 2D co-culture. This treatment also completely abolished the over-production of melanin, whose content was comparable to the control (Figure 4c).

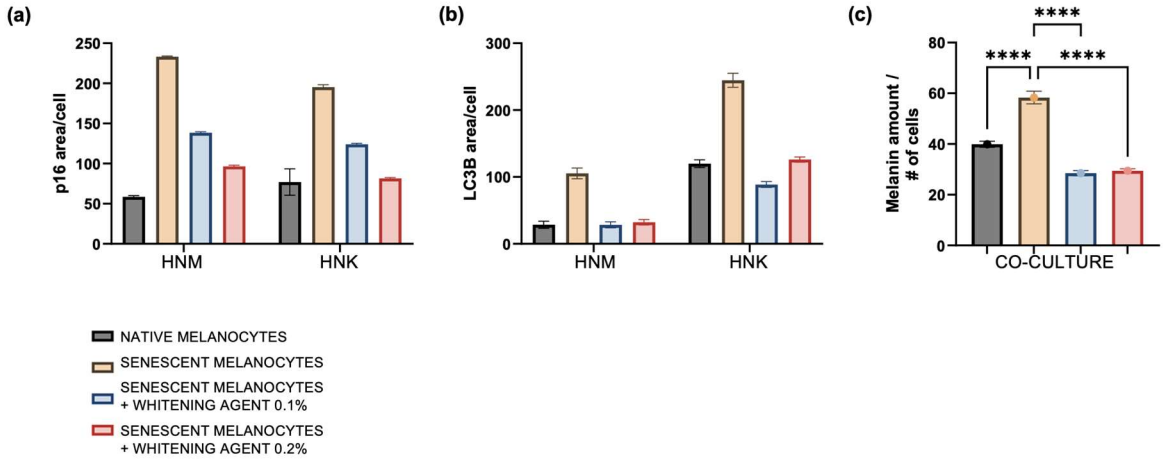

Figure 4. (a) Quantification of p16 levels in NHEM or NHEK in the indicated conditions. **(b)** Quantification of LC3B levels in NHEM or NHEK in the indicated conditions. **(c)** Quantification of melanin content in the co-culture.

3.4 Incorporation of UVA/UVB-induced senescence melanocytes in a 3D full-thickness skin model leads to a drastic increase of epidermal senescence and pigmentation which can be reversed by a whitening agent

To further examine the influence of menalocyte-related senescence on native keratinocyte in a more "*in-vivo* like" environment, we developed a 3D bioprinted full-thickness model incorporating UVA/UVB-induced senescence NHEM. Unexposed native NHEM were used as negative control. Histological analysis demonstrated that 3D skin constructs including senescent NHEM were well structured with an epidermal compartment fully differentiated from the *stratum basale* to the *stratum corneum* as assessed by HPS staining (Figure 5a). Remarkably, we observed that the epidermis was thinner with a significant decrease of the number of differentiated layers. Interestingly, $p16^{INK4a}$ expression was drastically increased in epidermal keratinocytes of 3D bioprinted skin model incorporating senescent NHEM compared with the models engineered with native NHEM (Figure 5 b). p16 expression epidermal profil showed a clear gradient of intensity from the basal to the suprabasal layers suggesting a clear paracrine effect of senescent NHEM located in the basal layer close to the neighbouring keratinocytes. Pigmentation was then assessed with a Warthin-Starry staining, which revealed a +75% melanin in skin prepared with UV-induced senescent melanocytes compared to the control (Figure 5 a,c). The number of melanocytes scored in both skin models was similar confirming the activation of the melanogenese and excluding an activation of the melanocyte proliferation (Figure 5 a,d).

3D bioprinted skin models incorporating senescent NHEM were treated with an active ingredient, known for its whitening properties, applied in a systemic way along the culture. Immunohistological analysis demonstrated that such treatment significantly decreased the expression of p16-positive epidermal cells compared with the untreated control. This decline is accompagnied by a clear decrease of the pigmentation without affecting the number of Melan-A positive cells.

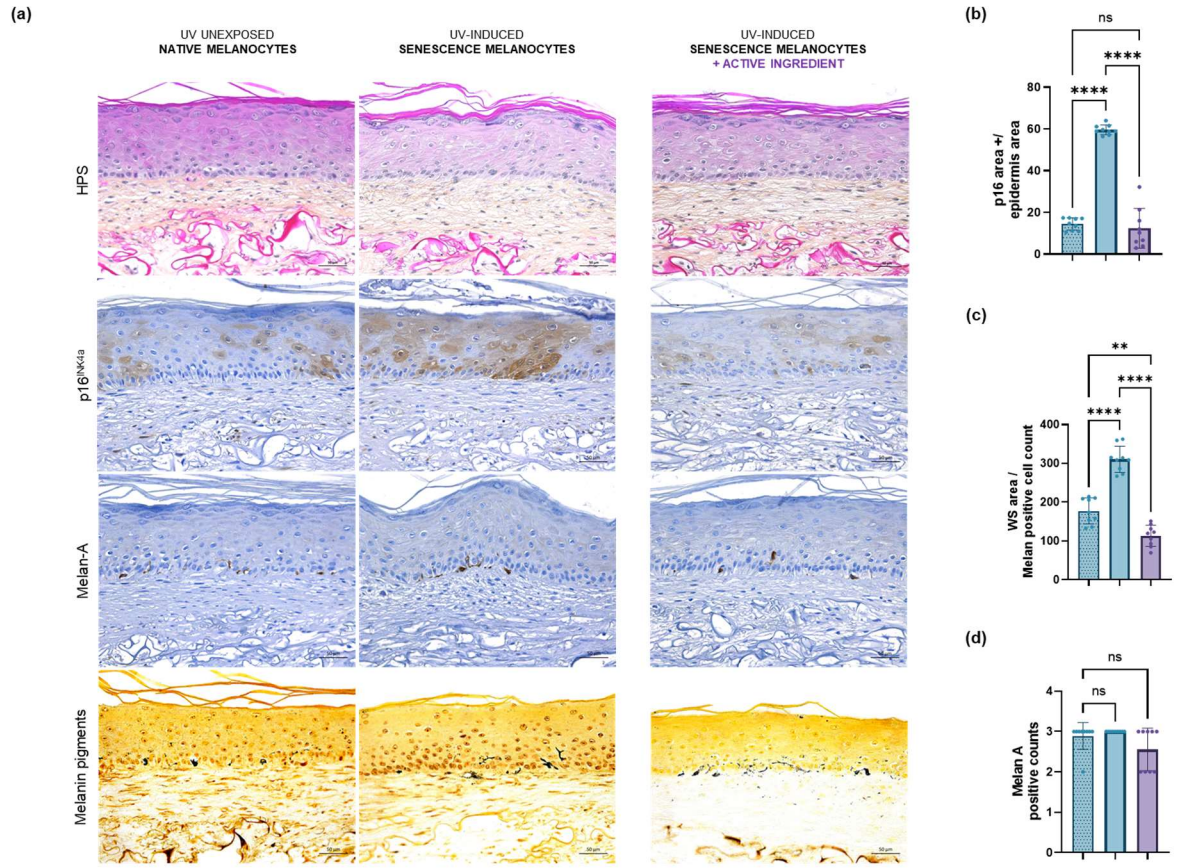

Figure 5. (a) Histological and immunohistological analysis of 3D bioprinted pigmented full-tickness skin model incorprating UVA/B-senescence induced NHEM treated or not with an active ingredient. Quantification of **(a)** p16 levels, **(b)** pigmentation and **(c)** Melan-A expression in 3D skin model engineered with native or senescent NHEM.

4. Discussion

To date, very few publications link melanocyte senescence and pigmentation defects, despite the fact that melanocytes were shown to be the main epidermal senescent cell population *in vivo* **[5,8]**. Here, we used both 2D and 3D skin models to further characterize how senescent melanocytes convey their deleterious message to neighbouring keratinocytes, and how this impacts melanin production. $p16^{INK4A}$ is the primary driver of replicative senescence of melanocytes **[9]**. We used this well described senescent marker to assess the impact of different combinations of UVA and UVB in melanocyte cultures and choose the best conditions for the rest of the study. Our study did not only assess the direct impact of UV exposure, but rather its long-term consequences. Indeed, p16 levels were still high up to two weeks after the last exposure, similar to what was observed in a previous study using UVB irradiation **[10]**. These results suggest that p16 is important for the maintenance of senescence in melanocytes. In addition, we observed that exposed melanocytes activate the autophagy pathway. As autophagy regulates cellular turnover by disassembling its dysfunctional constituents, its activation following UV exposure suggest that melanocytes engage in the activation of a stress response. Autophagy is thought to induce melangenesis and regulate melanosome biogenesis in

melanocytes **[11]** . While we did observe an UV-dependent increase in melanin content, activation of autophagy with the mTOR inhibitor Rapamycin did not. The function of autophagy activation in melanin production remains to be investigated in our system. Moving to our 3D skin model, we observed that tissue reconstruction with senescent melanocytes did not prevent their proper integration in the epidermal basal layer. This confirms that senescent is a viable state and that the cells are sill metabolically active. Their presence induced a wave of p16 that could be observed from the epidermal basal to the more differentiated top layers. In addition, melanin content was increased, suggesting that even 2 weeks following the last UV exposure these melanocytes were still over-producing melanin pigments. Our 3D skin model also highlighted the presence of melanin pigments below the dermal-epidermal junction. This is reminiscent of "*incontinentia pigmenti*", a rare disorder that results in the inability of the dermal-epidermal junction to retain melanin pigments in the epidermis. This phenotype can also be seen with skin aging, as the dermal-epidermal junction flattens and becomes less organized, which can also make it easier for melanin to leak into the dermis and create age spots.

5. Conclusion

Our results strongly support senescent melanocytes as a key driver of human skin pigmentation defects in a 3D full-thickness model. We demonstrate a strong paracrine effect of senescent melanocytes to neighbouring keratinocytes, leading to deleterious consequences in 2D and in 3D skin models. Furthermore, we have shown that our 3D model incorporating senescent melanocytes provides an excellent system for modeling age hyperpigmentary spots. In addition, our work establishes a robust platform for screening ingredients with the potential to prevent pigmentation disorders, for incorporation into anti-aging cosmetic formulations.

1. Cichorek, M. et al. Adv. Dermatol. Allergol.Postępy Dermatol. Alergol. 2013, 30, 30–41, doi:10.5114/pdia.2013.33376.
2. Fitzpatrick, t.b.; Breathnach, a.s. Dermatol. Wochenschr. 1963, 147, 481–489.
3. Thingnes, J. et al. PLoS ONE 2012, 7, e40377, doi:10.1371/journal.pone.0040377.
4. Whiteman, D.C. et al. Arch. Dermatol. Res. 1999, 291, 511–516, doi:10.1007/s004030050446.
5. Victorelli, S. et al. Embo J 2019, 38, e101982, doi:10.15252/embj.2019101982.
6. Martic, I. et al. Mech Ageing Dev 2020, 190, 111322, doi:10.1016/j.mad.2020.111322.
7. Santos, M.D. et al. Matrix Biol 2015, 47, 85–97, doi:10.1016/j.matbio.2015.03.009.
8. Hughes, B.K.; et al. Ageing. Biomed 2022, 10, 3111, doi:10.3390/biomedicines10123111.
9. Sviderskaya, E.V. et al. J. Natl. Cancer Inst. 2002, 94, 446–454, doi:10.1093/jnci/94.6.446.
10. Choi, S.-Y. et al. J. Dermatol. Sci. 2018, 90, 303–312, doi:10.1016/j.jdermsci.2018.02.016.
11. Kim, J.Y. et al. Pigment Cell Melanoma Res. 2020, 33, 403–415, doi:10.1111/pcmr.12838.